Deformation rates from faulting at the Tempe Terra extensional province, Mars

Scott J. Wilkins[1] and Richard A. Schultz
Geomechanics-Rock Fracture Group, Department of Geological Sciences, University of Nevada, Reno, Nevada, USA

Robert C. Anderson
Jet Propulsion Laboratory, Pasadena, California, USA

James M. Dohm
Department of Hydrology and Water Resources, University of Arizona, Tucson, Arizona, USA

Nancye H. Dawers
Department of Geology, Tulane University, New Orleans, Louisiana, USA

Received 26 April 2002; revised 13 June 2002; accepted 25 June 2002; published 25 September 2002.

[1] Rates of deformation are estimated from exposed normal faults within the Tempe Terra extensional province, Mars, through an analysis that incorporates fault segment linkage and utilizes regional observations of displacement-length relationships measured from Mars Orbiter Laser Altimeter topographic data. Moment rates (from 10^{14}–10^{16} N-m/yr), strain rates (10^{-12}–10^{-11} yr^{-1}) and rifting velocities (~0.003 mm/yr) are comparable to rates of deformation on stable plate interiors of Earth. The calculated low rates of rifting may result from the poorly constrained timing of deformation on Mars. Cumulative moment release estimates decrease linearly with time from Noachian (~1×10^{25} N-m) to Early Hesperian (~6×10^{24} N-m) and Late Hesperian-Early Amazonian (~1×10^{24}). These results indicate that a portion of Tharsis-related deformation remained localized within the Tempe Rift throughout much of Martian history, and provide important constraints for models of Martian mantle convection. *INDEX TERMS:* 5475 Planetology: Solid Surface Planets: Tectonics (8149); 6225 Planetology: Solar System Objects: Mars; 8010 Structural Geology: Fractures and faults; 8109 Tectonophysics: Continental tectonics—extensional (0905); 8155 Tectonophysics: Evolution of the Earth: Plate motions—general. **Citation:** Wilkins, S. J., R. A. Schultz, R. C. Anderson, J. M. Dohm, and N. H. Dawers, Deformation rates from faulting at the Tempe Terra extensional province, Mars, *Geophys. Res. Lett.*, *29*(18), 1884, doi:10.1029/2002GL015391, 2002.

1. Introduction

[2] The purpose of this contribution is to characterize the fault population statistics in order to quantify the spatio-temporal evolution of fault-related deformation at the Tempe Terra extensional province, Mars: a localized system of normal faults and grabens that has characteristics comparable to narrow continental rifts on Earth [*Hauber and Kronberg*, 2001]. Tempe Terra comprises a plateau of densely cratered and faulted Noachian terrains and moderately faulted younger sequences of Hesperian and upper Amazonian volcanics [*Scott and Tanaka*, 1986; *Anderson et al.*, 2001] situated on the northeastern edge of Tharsis: a region of concentrated faulting and volcanic activity that encompasses the western hemisphere of Mars [e.g., *Solomon and Head*, 1982]. Although regional fault maps have been used to qualitatively portray the spatio-temporal variations in tectonic activity surrounding Tharsis [*Anderson et al.*, 2001], quantities necessary to characterize the deformation and associated surface motions, including moments, strain rates, and rift velocities, have not previously been estimated using Mars Orbiter Laser Altimeter (MOLA) topographic data. Surface motions are manifestations of mechanical work obtained through thermal convection in the mantle, and therefore represent fundamental quantities necessary to determine thermodynamic characteristics of the Martian interior [e.g., *Harder*, 2000].

[3] In this paper we characterize the fault length population at Tempe Terra by revising previous regional fault trace maps (2426 independent segments) produced from 1:2,000,000 scale Mars Digital Image Mosaics and geological maps [*Scott and Tanaka*, 1986], which include information on relative timing [*Anderson et al.*, 2001], to incorporate effects of segment linkage. We then establish displacement-length scaling relations of grabens with MOLA data, and use these data to calculate rates of deformation in this region. We find that extension apparently persisted at Tempe Terra throughout much of Martian history, with average rates of deformation two orders of magnitude less than those from rifts on Earth.

2. Approach

[4] The technique we employ for calculating fault related strain rates, cumulative moments, and rifting velocities builds on previous approaches [e.g., *Scholz and Cowie*, 1990; *Marrett and Allmendinger*, 1991] that entail the analysis of fault displacements (d) and lengths (l), and relies on the observation that maximum displacements are proportional to fault lengths within a region ($d_{max} = \gamma l$) [*Clark and Cox*, 1996]. To avoid measuring displacements on all faults within Tempe Terra, we use the observed relationship between d_{max} and l measured from released MOLA topography (as of March 2002), and establish $d_{max} = \gamma l$ for the region. We use the conversion $d_{avg} \approx 0.67\ d_{max}$, which is consistent with

[1]Now at Shell EP Technology and Research.

0094-8276/02/2002GL015391$05.00

inelastic models of faulting [*Moore and Schultz*, 1999], so that we can calculate the geologic (cumulative vs. seismic or incremental) moment ($M_o = GAd_{avg}$; G is shear modulus, A is fault area [$l \times w$]): a quantitative representation of the total mechanical work done by faulting. With the *d-l* relations described above, the geologic moment tensor [M_{ij}, *Aki and Richards*, 1980, p. 117–118] for all faults within the specified region is,

$$\sum M_{ij}^k = 0.67\gamma\left(l^k\right)^2\left(d_i^k n_j^k + d_j^k n_i^k\right)G(w/\sin\theta). \qquad (1)$$

where d and n are unit vectors of displacement and the normal to the kth fault, respectively, w is the maximum depth of faulting, and θ is fault dip. We divide (1) by time (t) to calculate moment rates, calculate strain rates with $\dot{\varepsilon}_{ij}^{Y} = \Sigma M_{ij}^k / 2GVt$ (for symmetrical, irrotational strain; *Molnar* [1983]; V is volume) and relative velocities of rifting by multiplying each component of strain rate by the length of the respective direction (e.g., $v_{yy} = l_y \varepsilon_{yy}^{Y}$, *Jackson and McKenzie* [1988]). The asymmetric moment tensor is not used because most normal faults at Tempe occur in parallel, graben forming pairs that exhibit symmetrical displacements, and thus act to cancel any rotational element [*Molnar*, 1983].

[5] In this analysis, a significant source of uncertainty in strain rates stems from the assessment of fault lengths. Closely spaced échelon fault segments can interact mechanically to form a single, kinematically coherent fault [e.g., *Dawers and Anders*, 1995]. Importantly, d_{max}/l is modulated during the process of segment linkage [*Cartwright et al.*, 1995], thus requiring careful calibration of d_{max} to l to establish γ in (1). Displacements and displacement gradients increase in response to increased magnitudes of local driving stress in the vicinity of adjacent, mechanically interacting faults [*Willemse*, 1997; *Gupta and Scholz*, 2000]. The critical degree of interaction necessary for segment linkage is associated with the ratio between separation (s) and overlap (o) of the independent fault segments relative to the spacing between fault midpoints ($2k$) [*Gupta and Scholz*, 2000; *Schultz*, 2000]. We define critical values of relative overlap ($0 < o/k < 0.5$) and separation ($0 < s/k < 0.1–0.2$) for linkage, consistent with observations from both terrestrial and Martian fault studies [*Gupta and Scholz*, 2000; *Schultz*, 2000].

3. Fault Length Populations

[6] The cumulative frequencies of both independent (i.e., mapped) and linked fault length populations are normalized by the *2-D* area of the investigation for each Martian epoch (Figure 1) and displayed in Figure 2. The fault lengths are displayed as a function of age (Figure 2a) and linkage criterion values (Figure 2b) to illustrate differences in strain as a function of these parameters. The number of faults decreases from Noachian to Late Hesperian - Early Amazonian (LH-EA) times (Figure 2a; see web Table 1 for time scales[1], and this pattern is not dependent on the linkage values invoked. Segment linkage increases fault lengths while reducing the total number of faults within the population

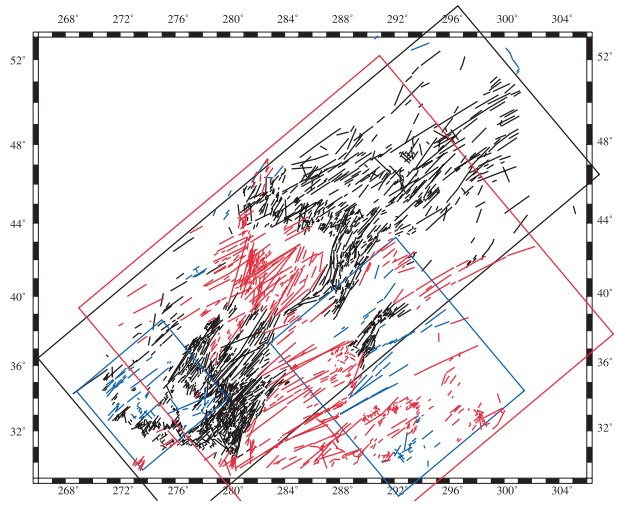

Figure 1. Noachian (black), Early Hesperian (red), and Late Hesperian-Early Amazonian (blue) fault trace maps at Tempe Terra for linked faults with $0 < o/k < 0.5$ and $0 < s/k < 0.1$. Areas used for strain and velocity calculations (colored boxes) are listed in Web Table 1.

(Figure 2b). This result is consistent with theoretical fault growth models where segment linkage increases the average lengths of the population, leading to an increase in strain and a reduction in the power-law exponent (slope of the frequency-length curve, Figure 2) [*Cowie et al.*, 1995; *Cladouhos and Marrett*, 1996]. Using the segment linkage criterion, the greatest increase in fault lengths is apparent only for the largest faults, which is consistent with the idea of progressive localization of the population strain onto the largest faults [*Cowie et al.*, 1995; *Cladouhos and Marrett*, 1996].

[7] If the entire population follows a single power-law distribution (i.e., constant slope in Figure 2), the frequency of fault lengths <~30 km is significantly less than that predicted from the distribution of lengths >~30 km. This difference has been assumed to result from sampling biases: some percentage of faults are not exposed at the surface because when distributed in three dimensions they are too small to span the faulted layer [e.g., *Marrett and Allmendinger*, 1991]. To correct for this *apparent* discrepancy, many researchers extrapolate the population statistics from the larger faults to predict the number of unobserved small faults [e.g., *Scholz and Cowie*, 1990; *Marrett and Allmendinger*, 1991], which is analogous to projecting the frequency-magnitude relation of earthquakes. However, because this extrapolation to 3-D spatial distributions can be problematic for natural fault populations [*Borgos et al.*, 2000], we use the measured (and linked) length distributions in all calculations so that our estimates of deformation thus represent *minimum* magnitudes. The small faults (<15 km) contribute relatively insignificant amounts (<8%) to the total deformation at the current stage of fault population development, and indicate that deformation estimates should not be significantly increased to account for the presence of blind faults.

4. Displacement-Length Scaling

[8] Maximum vertical relief is measured along topographic profiles perpendicular to fault strike (from a DEM

[1] Supporting material is available via Web browser or via Anonymous FTP from ftp://ftp.agu.org, directory "apend" (Username = "anonymous", Password = "guest"); subdirectories in the ftp site are arranged by paper number. Information on searching and submitting electronic supplements is found a http://www.agu.org/pubs/esupp_about.html.

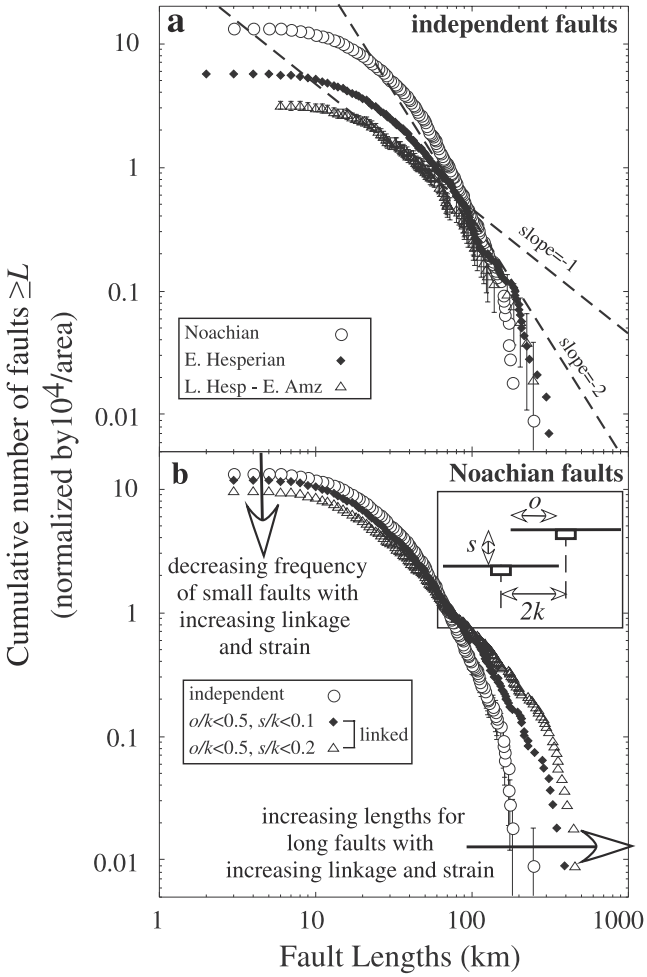

Figure 2. Cumulative frequency of fault lengths at Tempe Terra as a function of (a) age for mapped (independent) faults and (b) linkage (o/k < 0.5 and s/k < 0.1–0.2) for Noachian aged faults.

of the region gridded at ~256 pixels/degree) on both linked and isolated fault segments with lengths ranging from ~10–350 km. We associate vertical relief with a minimum magnitude of fault throw because offset hanging wall materials appear covered with younger sediments and the possibility of footwall erosion. We assume all displacements are dip-slip because geomorphic or structural evidence for strike-slip components of displacement, such as laterally offset erosional features (i.e., gullies, shutter ridges, or slide deposits), subsidiary echelon fold/fault systems associated with larger faults, or extension/contraction structures at fault bends and stepovers are not found in any images. For lengths of ~10–350 km and a 60° dip, $d_{max} = 0.0067l^{0.969}$ ($R^2 = 0.66$) for 58 faults that exhibit the clearest displacement distributions and fault tips within the region (Figure 3). A ten-degree variation in fault dip (from 60°, a common range for Earth), results in insignificant changes (<±0.0006) in d_{max}/l.

5. Geologic Moment Rates, Strain Rates, and Rifting Velocities

[9] Web Table 1 summarizes the deformation at Tempe Terra for both independent and linked fault populations, with $0 < o/k < 0.5$ and $0 < s/k < 0.1–0.2$. The calculations utilize $\gamma = 0.0067$ for a $\theta = 60°$, the fault lengths displayed in Figure 2, a 15 km depth of faulting (w = **z**, see Web Table 1 for coordinate conventions) that is consistent with mechanical models of fault related topography for the central Tempe Rift [*Wilkins et al.*, 2000], G representative of average crustal properties (3.3×10^{10} Pa), and an absolute Martian time scale from the most recent estimates (*Hartmann and Neukum* [2001]; Web Table 1).

[10] Geologic moment rates range from $10^{14}–10^{16}$ N-m/yr regardless of the linkage values used, although rates are higher for the largest critical separation value. Interestingly, these moment rates, calculated from normal faults at Tempe Terra, are similar to that calculated by *Golombek* [1992] for all structures within the entire (much larger) Tharsis province. *Golombek* [1992] used (1) constant displacements of 0.5 km for the Tempe Rift and 0.3 km for "simple" grabens (with no *d-l* relationship), (2) a shallower depth of faulting, and (3) a smaller shear modulus than is used here. We suggest that the previous values for Tharsis moment rates substantially underestimate the actual values for the province, mostly due to smaller estimates of the first two parameters listed above.

[11] Cumulative strain rates at Tempe Terra are found to range from $10^{-12}–10^{-11}$ yr^{-1}. Strain rates in the **z** and **y** directions, oriented vertical and perpendicular (140°–320°) to the mean trend of the rift axis (050°–230°), respectively, are the two largest components (Web Table 1). The data indicate that the deformation is dominated by crustal thinning, and secondarily by extension perpendicular to the rift axis. The dominance of crustal thinning results from variation in fault trend relative to **y** and not assumptions concerning fault dip. The relative velocity of rifting is largest for Hesperian time (0.04–0.06 mm/yr), and averages ~0.0029 mm/yr for the full time of the deformation. These strain rates and

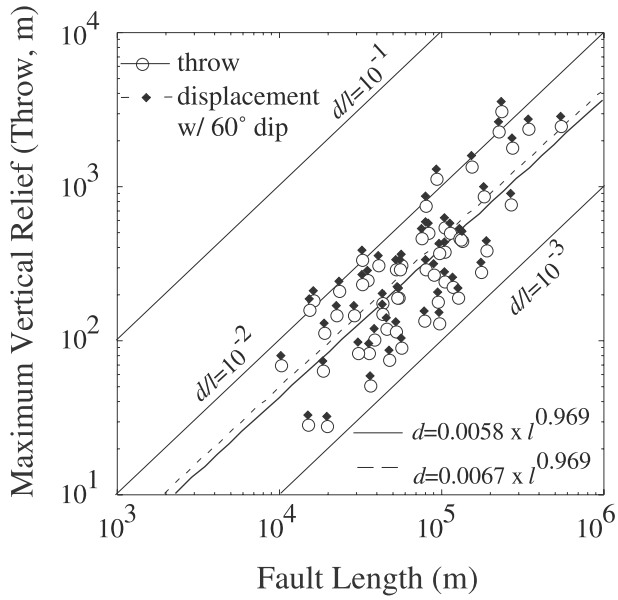

Figure 3. Maximum structural relief (throw) vs. fault length for grabens at Tempe Terra (circles) and power-law fit (solid line). Trigonometric correction for fault dips of 60° (solid diamonds) display little difference in d/l from throw/l. Dashed line represents power-law fit of displacements to length.

velocities are comparable to those from stable plate interiors on Earth [e.g., *Gordon*, 1998].

6. Discussion and Conclusions

[12] The Martian time-stratigraphic system is constructed from a combination of relative stratigraphic dating [e.g., *Scott and Tanaka*, 1986] and measurements of the relative density of impact craters on the exposed surfaces, that is then used to calculate absolute ages based on estimates of crater flux rates [e.g., *Hartmann and Neukum*, 2001]. Uncertainty in estimated impact crater retention ages results in errors that could be as large as a factor of two [*Hartmann and Neukum*, 2001]. The morphology of most of Tempe Terra is similar to that of narrow rifts on Earth [*Hauber and Kronberg*, 2001], yet the moment estimates and strain rates are extremely slow, and comparable to rates of deformation measured on stable plate interiors [*Gordon*, 1998]. *Buck* [1991], in a compilation of extension velocities from narrow continental rifts on Earth, found velocities of 0.1–0.7 cm/yr, two orders of magnitude larger than the fastest velocity of extension that we calculated in this paper. Furthermore, *Buck* [1991] calculated a wide range of plausible strain rates (10^{-5}–10^{-10} yr^{-1}), which are dependent on Moho temperature, heat flux, and rheology. These estimates are also faster than the strain rates calculated here, and, taken at face value, would suggest that rift processes are slower on Mars than on Earth. Alternatively, the rate differences may result from a combination of an unreliable absolute time-scale for Mars and a lack of detailed distinction among stratigraphic units (K.L. Tanaka, personal communication, 2002).

[13] Regardless of the uncertainties in the timing of deformation, the temporal pattern of cumulative moment release provides quantitative constraints on models of Tharsis development. Cumulative moment estimates decrease linearly with time from Noachian ($\sim 1 \times 10^{25}$ N-m) to Early Hesperian ($\sim 6 \times 10^{24}$ N-m) and Late Hesperian-Early Amazonian ($\sim 1 \times 10^{24}$ N-m) at Tempe Terra, indicating that either Tharsis related deformation waned at an apparently constant rate, or perhaps a larger fraction of the deformation occurred later in Martian history (i.e., Hesperian-Amazonian) but cannot be detected because of the lack of stratigraphic constraints (e.g., some faults only displace Noachian terrain).

[14] We estimate minimum velocities of rifting and crustal thinning to be $\sim 10^{-2}$–10^{-3} and $\sim 10^{-4}$ mm/yr, respectively. *Harder* [2000] suggested that the geometry of mantle convection and surface velocities will vary depending on mantle chemistry and rheology, but average surface velocities of 25 mm/yr are predicted if an endothermic phase transition to perovskite exists near the Martian core-mantle boundary, whereas much higher rates (and shorter wavelength convection) would occur otherwise. Although this would be consistent with rates of rifting on Earth, it is ~2 orders of magnitude faster than we estimate here. Despite the stated uncertainties in rate estimates, the values for Tempe demonstrate a persistent, slow deformation rate in this region of Tharsis.

[15] **Acknowledgments.** This work was supported by NASA's Mars Data Analysis Program (grant to R.A. Schultz). We thank D. A. Ferrill, S. A. Kattenhorn, and R. A. Schweickert for thorough reviews that sharpened the final paper.

References

Aki, K., and P. G. Richards, *Quantitative Seismology: Theory and Methods*, 932 p., W. H. Freeman, San Francisco, California, 1980.

Anderson, R. C., J. M. Dohm, M. P. Golombek, A. F. C. Haldemann, B. J. Franklin, K. L. Tanaka, J. Lias, and B. Peer, Primary centers and secondary concentrations of tectonic activity through time for the western hemisphere of Mars, *J. Geophys. Res.*, *106*, 20,563–20,585, 2001.

Borgos, H. G., P. A. Cowie, and N. H. Dawers, Practicalities of extrapolating one-dimensional fault and fracture size-frequency distributions to higher-dimensional samples, *J. Geophys. Res.*, *105*, 28,377–28,391, 2000.

Buck, W. R., Modes of continental lithospheric extension, *J. Geophys. Res.*, *96*, 20,161–20,178, 1991.

Cartwright, J. A., B. D. Trudgill, and C. M. Mansfield, Fault growth by segment linkage: An explanation for scatter in maximum displacement and trace length data from the Canyonlands Grabens of S. E. Utah, *J. Struct. Geol.*, *17*, 1319–1326, 1995.

Cladouhos, T. T., and R. Marrett, Are fault growth and linkage models consistent with power-law distributions of fault lengths?, *J. Struct. Geol.*, *18*, 281–293, 1996.

Clark, R. M., and S. J. D. Cox, A modern regression approach to determining fault displacement-length scaling relationships, *J. Struct. Geol.*, *18*, 147–152, 1996.

Cowie, P. A., D. Sornette, and C. Vanneste, Multifractal scaling properties of a growing fault population, *Geophys. J. Int.*, *122*, 457–469, 1995.

Dawers, N. H., and M. H. Anders, Displacement-length scaling and fault linkage, *J. Struct. Geol.*, *17*, 607–614, 1995.

Golombek, M. P., A prediction of Mars seismicity from surface faulting, *Science*, *258*, 979–981, 1992.

Gordon, R. G., The plate tectonic approximation: Plate nonrigidity, diffuse plate boundaries, and global plate reconstructions, *Annu. Rev. Earth Planet. Sci.*, *26*, 615–642, 1998.

Gupta, A., and C. H. Scholz, A model of normal fault interaction based on observations and theory, *J. Struct. Geol.*, *22*, 865–879, 2000.

Hartmann, W., and G. Neukum, Cratering chronology and the evolution of Mars, *Space Sci. Rev.*, *96*, 1–30, 2001.

Harder, H., Mantle convection and the dynamic geoid of Mars, *Geophys. Res. Let.*, *27*, 301–304, 2000.

Hauber, E., and P. Kronberg, Tempe Fossae, Mars: A planetary analogon to a terrestrial continental rift?, *J. Geophys. Res.*, *106*, 20,587–20,602, 2001.

Jackson, J., and D. McKenzie, The relationship between plate motions and seismic moment tensors, and the rates of active deformation in the Mediterranean and Middle East, *Geophys. J.*, *93*, 45–73, 1988.

Marrett, R., and R. W. Allmendinger, Estimates of strain due to brittle faulting: Sampling of fault populations, *J. Struct. Geol.*, *13*, 735–738, 1991.

Molnar, P., Average regional strain due to slip on numerous faults of different orientations, *J. Geophys. Res.*, *88*, 6430–6432, 1983.

Moore, J. M., and R. A. Schultz, Processes of faulting in jointed rocks of Canyonlands National Park, Utah, *Geol. Soc. Amer. Bull.*, *111*, 808–822, 1999.

Scholz, C. H., and P. A. Cowie, Determination of total geologic strain from faulting, *Nature*, *346*, 837–839, 1990.

Schultz, R. A., Fault-population statistics at the Valles Marineris extensional province, Mars: Implications for segment linkage, crustal strains, and its geodynamical development, *Tectonophysics*, *316*, 169–193, 2000.

Scott, D. H., and K. L. Tanaka, Geologic Map of the Western Equatorial Region of Mars, scale 1:15,000,000, *U.S.G.S. Misc. Invest. Ser. Map, I-1802-A*, 1986.

Solomon, S. C., and J. W. Head, Evolution of the Tharsis province of Mars: The importance of heterogeneous lithospheric thickness and volcanic construction, *J. Geophys. Res.*, *87*, 9755–9774, 1982.

Wilkins, S. J., R. A. Schultz, and H. Frey, Displacement-length relationships of grabens in Tempe Terra, Mars (abstract), *Am. Geophys. Union*, Fall, 2000.

Willemse, E. J. M., Segmented normal faults: Correspondence between three-dimensional mechanical models and field data, *J. Geophys. Res.*, *102*, 675–692, 1997.

R. C. Anderson, Jet Propulsion Laboratory, California Institute of Technology, 4800 Oak Grove Drive, Pasadena, California 91109, USA. (R.C.Anderson@jpl.nasa.gov)

N. H. Dawers, Department of Geology, Tulane University, New Orleans, Louisiana, 70118 USA. (ndawers@tulane.edu)

J. M. Dohm, Department of Hydrology and Water Resources, University of Arizona, Tucson, Arizona, 85721 USA. (jmd@hwr.arizona.edu)

R. A. Schultz and S. J. Wilkins, Geomechanics-Rock Fracture Group, Department of Geological Sciences, University of Nevada, Reno, Nevada, 89557-0138 USA. (swilki@unr.edu; schultz@mines.unr.edu)